ELSEVIER

Chemical Engineering Science 61 (2006) 5500–5514

Chemical Engineering Science

www.elsevier.com/locate/ces

Effects of interfacial surfactant contamination on bubble gas transfer

Diego Rosso*, Derry L. Huo, Michael K. Stenstrom

Henri Samueli School of Engineering and Applied Science, University of California, Los Angeles, CA 90095, USA

Received 12 August 2005; received in revised form 28 March 2006; accepted 14 April 2006
Available online 28 April 2006

Abstract

Surface active agents depress gas transfer at gas–liquid interfaces. They are present as measurable trace contaminants at all environmental and at most industrial interfaces. An experimental apparatus to concurrently measure dynamic surface tension and mass transfer was constructed and tested for single-bubble and multi-bubble experiments. In this work, the parameters describing time-dependent bubble surface contamination were characterized. The application of a Ward–Tordai transient model and of a Langmuir saturation model showed that for fine-bubbles in low molecular weight surfactant solutions the interfacial surfactant accumulation equilibrates before bubble detachment. This is reflected in the bubbles behaving as solid-spheres, which is shown in our dimensionless results.

For a given contamination, interfaces with higher renewal rates have higher mass transfer. At higher renewal rates, the variation due to different contamination is smaller than the variation at lower renewal rates, concluding that higher interfacial flow regimes can offset contamination. Our experimental evidence shows a gas transfer reduction of 30–70% of pure water values in surfactant solutions, which confirms full-scale field measurements. Results are consistent with expectations and correct previous Frössling-like dimensionless correlations for pure water systems. Our results offer a tool for mass transfer prediction from flow regime and surfactant properties.

Keywords: Adsorption; Aeration; Bubble; Gas–liquid interface; Mass transfer; Surfactant

1. Introduction

Gas–liquid reactors have extensive application in the industrial and environmental fields. Several technologies are available for generating gas–liquid interfaces. Aeration devices transfer gas to liquid media by either creating a gas–liquid interface or using a semi-permeable membrane that allows the dissolution of gas in the liquid without the formation of an interface. Environmental applications usually rely on the former method, where the gas–liquid interface is created by either shearing the liquid surface with a mixer or turbine, or by releasing air through spargers (producing coarse bubbles), porous sintered ceramic materials or punched polymeric membranes (producing midrange or fine bubbles, according to ceramic granulometry and gas flowrate). In environmental applications, it is customary to consider fine the bubbles with a diameter smaller than 5 mm. Coarse bubbles are larger and may have diameters as large as 50 mm. Porous sintered materials and polymeric punched membranes are usually referred to as fine pore diffusers. Novel technologies (referred to as bubbleless) adopt "true" semi-permeable membranes, such as membranes used for reverse osmosis, which allow the transport of water and air across the membrane, without permitting the passage of solute or suspended matter (Côté et al., 1989). This paper focuses on fine-bubble gas–liquid interfaces.

Environmental processes are characterized by the presence of a variety of contaminants, both hydrophobic and hydrophilic. The most frequently occurring contaminants accumulating at environmental interfaces are surface active agents, also referred to as surfactants. Commercially available surfactants are key components of soaps and detergents and have a dual chemical nature, with a polar (hydrophilic) head and a hydrophobic tail. Due to their amphiphilic nature, they accumulate at the interface of aqueous-gaseous systems and lower the gas–liquid interfacial tension. The interfacial tension decreases with increasing surfactant concentration, until the critical micelle concentration (CMC) is reached. The CMC corresponds to the formation in the aqueous solution of the first dispersed micelle. Surfactant concentrations above CMC show no change in interfacial

* Corresponding author: Tel.: +1 310 825 1408; fax: +1 310 206 2222.
E-mail address: bidui@ucla.edu (D. Rosso).

0009-2509/$ - see front matter © 2006 Elsevier Ltd. All rights reserved.
doi:10.1016/j.ces.2006.04.018

tension, as the surfactant excess concentration is present in the system as micelles.

The interfacial surfactant accumulation is a time-dependent phenomenon, and is the cause of time-dependent variation of interfacial tension. This variation is usually defined as dynamic surface tension (DST). Surfactant accumulation at contaminated bubble interfaces is characterized by the accumulation of hydrophilic heads at the gas–liquid interface, and the arrangement of the hydrophobic tails inside the bubble volume, occurring by chemical exclusion (Rosen, 1978). By covering part of the bubble surface, surfactants increase surface rigidity, and the bubble drag coefficient increases, approaching that of a rigid sphere, and resulting in diminished terminal velocity (Haberman and Morton, 1953; Alves et al., 2005). Furthermore, the presence of hydrophobic tails inside the bubble reduces the internal gas circulation, which reduces renewal of the gas-side mass transfer film (Garner and Hammerton, 1954). Boussinesq (1913) first proposed that the reduction in internal gas circulation in bubbles and drops is due to the interfacial accumulation of contaminants organized as a monolayer, which was validated experimentally by Garner and Hammerton (1954).

The interfacial shear generated by rising bubbles causes the accumulation of surfactants at the bubble rear, usually referred to as stagnant-cap. Evidence supports the existence of fore-and-aft symmetry in the interfacial concentration field (Clift et al., 1978; Fan and Tsuchiya, 1990). Several mass transfer models utilized the stagnant-cap hypothesis with success (e.g. Griffith, 1960; Weber, 1975; Sadhal and Johnson, 1983; Vasconcelos et al., 2002). In case of surfaces moving at high shear rates in highly contaminated liquids or with interfacial temperature gradients, surface concentration gradients are established, leading to countercurrent interfacial liquid circulation, known as the Marangoni effect (Marangoni, 1871). The data sets used in this study are isothermal and have surfactant concentration and interfacial shear magnitudes too low to experience Marangoni effects.

Mass transfer models for pure fluids are well-known and are based on the solid-sphere (Boussinesq, 1913) or the fluid sphere (Prandtl, 1934) approximation. Motarjemi and Jameson (1978) observed with experiments that mass transfer coefficients are higher than the predictions with the solid sphere model, indicating moving gas–liquid interfaces. The most common are the stagnant two-film model (Lewis and Whitman, 1924), the penetration theory (Higbie, 1935) and the surface renewal model (Danckwerts, 1951). Both the penetration theory and the surface renewal models account for the liquid agitation, doing so by embodying the flow regime parameters into the mass transfer calculation. Depending on the flow regime, these models can predict mass transfer of pure gas–liquid systems with accuracy. There also exist analytical solutions to the problem of mass transfer from falling pure spheres in laminar flow regime derived from the boundary layer theory (Friedlander, 1957).

The Lewis and Whitman model is extensively applied with success in evaluating aeration devices for environmental purposes (ASCE, 1984, 1991; ATV-DVWK, 1996; prEN 12255-15, 1999). The most common environmental application of aeration devices is supplying oxygen to aerobic bacterial colonies engineered to treat wastewater. When analyzing the efficiency of such processes, the mass transfer efficiency of aeration systems plays a key role. In the case of surface contamination, process mass transfer coefficients decrease to values well-below the ones measured in pure water (Mancy and Okun, 1960). Eckenfelder first investigated this phenomenon by measuring mass transfer coefficients in fine bubble aeration systems (Eckenfelder, 1959). His studies report experimental evidence that showed the overall mass transfer coefficient declining to 50% or less of the rate in pure water even though the high contamination produces larger interfacial areas (Eckenfelder and Barnhart, 1961).

In this paper, the effect of surfactant interfacial accumulation for fine-bubbles in gravitational flow is investigated. Both early and mature surface formation stages were included in the present research. Concurrent dynamic surface tension and mass transfer coefficient measurements were performed. Single-bubble and multi-bubble aeration apparatuses were built and tested. In this fashion, both time-dependent and time-averaged data were collected. Dynamic surface tension measurements were related to interfacial diffusivity, and this was related to mass transfer through empirical correlations. Previous empirical observations were confirmed and the effects of surfactant contamination can be quantified with corrections to Frössling-like correlations.

2. Materials and methods

Equilibrium surface tension was measured using both the capillary rise method and the Du Nuöy ring method (Lecomte du Noüy, 1919). The capillary apparatus used is from Fisher Scientific (Cat. No. 14-818), consisting of a 250 mm borosilicate glass capillary tube, graduated from 0 to 100 mm in 1 mm increments. The capillary radius of 0.35 mm was determined by measuring the surface tension of pure benzene in a thermostat-controlled bath at 20 and 40 °C. The Du Nuöy ring method depends upon the determination of the maximum pulling force necessary to detach a circular standardized ring of round wire from the surface of a liquid with a zero contact angle. Du Nuöy ring method measurements were performed using a Fisher Surface Tensiomat (Model 21), which is essentially a torsion balance. A Pt–Ir ring connected to a torsion arm is used to measure the surface detachment force. The Tensiomat was used in the semi-automatic mode to increase reproducibility. The apparent surface tension measurements collected with the ring method were converted to absolute values with the introduction of correction factors available in literature (Harkins and Jordan, 1930; Freud and Freud, 1930).

Dynamic surface tension measurements were collected with the maximum bubble pressure method (MBPM). A MBPM instrument was constructed in our laboratory and is illustrated in Fig. 1. In our set-up, the air tubing was passed through a desiccator (DRIERITE Gas Purifier, Model L68GP) to remove water vapour, which may cause pressure fluctuations. Downstream from an airflow meter (Cole Parmer, 0–7 ml min^{-1} scale) the air line was split into three lines. The first line was directed to a pressure transducer (Setra Systems, Model 264 D-10)

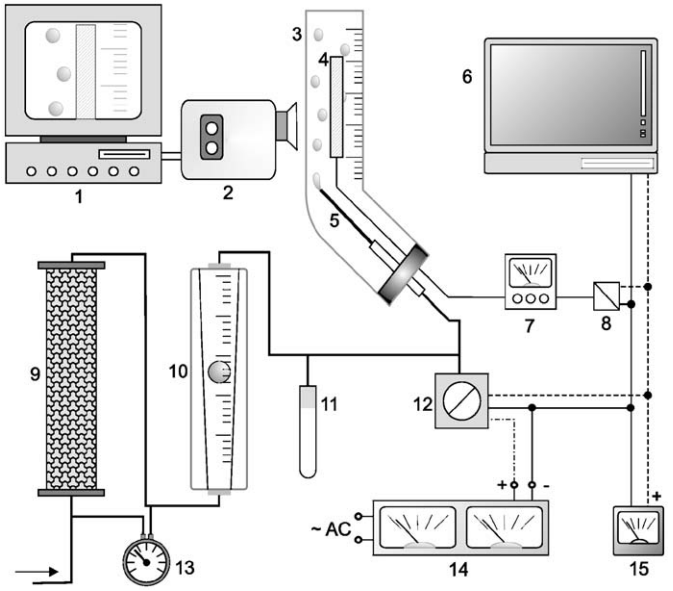

Fig. 1. Experimental apparatus: computer for image recording (1), camcorder (2), square graduated glass tube (3), micro-O_2 electrode (4), capillary needle (5), computer for signal logging (6), dissolved O_2 meter (7), A/D converter (8), desiccator (9), rotameter (10), buffer vial (11), pressure transducer (12), differential pressure gauge (13), power supply (14), voltmeter (15).

connected to a power supply. The pressure transducer senses the differential pressure inside the air line and converts it to a voltage for both unidirectional (0–10 V) and bi-directional (±5 V) pressure ranges. The second line is connected to a 40 ml glass vial serving as a gas buffer chamber. This vial helps maintain constant pressure in the air line through bubble formation and release. The third line is connected to a fused silica needle syringe with a Pyrex round capillary needle (Wilmad Glass, 0.15/0.25 mm internal/outer diameters, 100 mm long) releasing bubbles into a square graduated Pyrex glass tube with 0.1 mm scale subdivisions. The capillary needle points upwards and has an angle of 45 ° to the vertical. This reduces the bubble-life at high flowrates, because in a tilted needle system the buoyancy does not detach the bubble by tension, but also by shear, thus anticipating bubble detachment (Lin et al., 1994). Bubble diameters were measured by photographing the rising bubbles with a video camera operating at high shutter speed (1/10,000 shutter speed). Mathcad Plus was used to calculate bubble frequencies using a Fast Fourier Transform algorithm and a Visual Basic code was written and used to collect all data and calculate surface tension from voltage values.

A micro-O_2 electrode (Microelectrodes, Model MI-730) was placed inside the square graduated Pyrex glass tube. This was used to concurrently measure mass transfer coefficients while also recording DST and bubble diameters. Mass transfer measurements were performed by integrating the differential mass balance for the dissolved oxygen concentration x_{O_2} within the vial volume, assuming well-mixing:

$$\frac{dx_{O_2}}{dt} = k_L a \cdot (x_{O_2,\infty} - x_{O_2}), \tag{1}$$

over time to calculate the volumetric mass transfer coefficient $k_L a$ (time^{-1}) of the tested solution. The upper boundary of integration for Eq. (1) is the equilibrium concentration at saturation $x_{O_2,\infty}$. The solution to (1), assuming the initial condition:

$$x_{O_2} = x_{O_2,i} @\ t = 0$$

is

$$x_{O_2} = x_{O_2,\infty} - (x_{O_2,\infty} - x_{O_2,i})\, e^{-k_L a \cdot t}, \tag{2}$$

where $k_L a$ = overall mass transfer coefficient (T^{-1}), $x_{O_2,\infty}$ = equilibrium oxygen concentration at saturation = 9.08 mg l^{-1} @ $T = 20$ °C.

The error present in $k_L a$ estimated values can be minimized by using a composite predictive method, based on both exponential and logarithmic regression fits (Philichi and Stenstrom, 1989). This test consists initially in sequestrating the dissolved oxygen by oxidizing sodium sulphite to sodium sulphate with cobalt chloride as catalyzer, or

$$Na_2SO_3 + \frac{1}{2}O_2 \xrightarrow{CoCl_2} Na_2SO_4$$

and feeding O_2 to re-aerate the solution until saturation is finally reached. Fig. 1 shows the dissolved oxygen concentration time-series for a re-aeration test. If the air flowrate during the re-aeration process is kept constant, the series of bubbles released during the process will have uniform diameter distribution and the DST variability minimum. Oxygen concentrations and voltages in our tests were acquired via an analogue/digital converting board connected to a computer. This procedure is used in environmental engineering applications and is available in literature (ASCE, 1984, 1991; ATV-DVWK, 1996; prEN 12255-15, 1999).

The chemicals used in these tests were SDS (sodium *n*-dodecyl sulphate, $C_{12}H_{25}NaO_4S$, F.W. 288.38, CAS 151-21-3) and IAA (3-methyl-1-butanol or iso-amyl alcohol, $C_5H_{12}O$, F.W. 88.15, CAS 123-51-3). SDS, commercially known as sodium lauryl sulphate, is the most common surfactant present in soaps and detergents and is the most frequently occurring surfactant in wastewaters. Due to the variability of assay compositions, SDS from four different manufacturers were evaluated and the most consistent lot was used for all experiments. Iso-amyl alcohol was chosen because of its higher diffusivity and its lower molecular weight and volume. The deionized water used in this study was obtained with a Barnstead NANO pure Infinity ultrapure water system (resistivity, 18 MΩ cm).

Data from previous investigations in our laboratory are available and were included in this study (Masutani and Stenstrom, 1991; Huo, 1998). These included both time-dependent and time-averaged measurements. The time-dependent measurements were used to investigate and characterize contamination phenomena at gas–liquid interfaces, and were taken on sodium tetradecyl sulphate (TGT, under the Union Carbide trade name of Tergitol 4, $C_{14}H_{29}NaO_4S$, F.W. 316.43, CAS 1191-50-0) solutions with the same layout as shown in Fig. 2 . The time-scale of these measurements is absolute time. Time-averaged

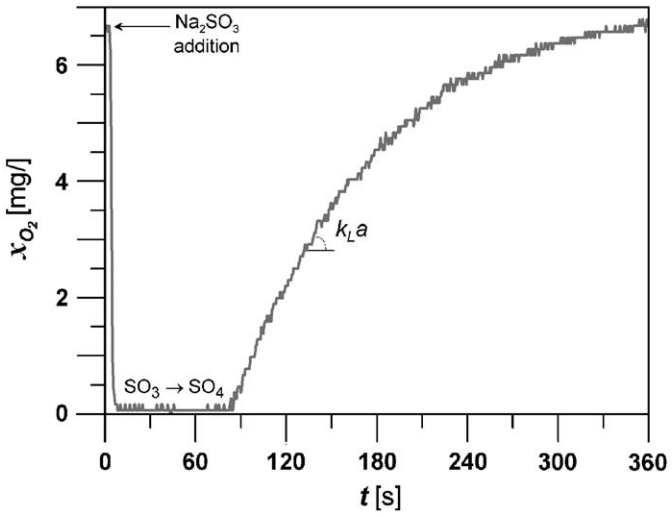

Fig. 2. Re-aeration test. The dissolved oxygen concentration x_{O_2} drops with the addition of Na_2SO_3 and starts increasing after the stoichiometric excess of sulphite is completely oxidized to sulphate. The derivative of the transient curve is proportional to the volumetric mass transfer coefficient $k_L a$.

measurements were used to apply the characterization of contamination phenomena to pilot-scale aeration reactors, and were performed on both SDS and TGT solutions in a 200 l diffused aeration vessel (Fig. 3). Fine bubbles were distributed through the bottom of the aeration vessel with a fine-pore ceramic diffuser at airflow rates of 8, 12, and 20 $l\,min^{-1}$. Two oxygen probes were used, and the results were averaged. The time-scale in these tests was the bubble age, i.e. the hydraulic retention time of bubbles in the vessel.

3. Theoretical basis

The goal of this study is to quantify in a dimensionless form the effect of gas-transfer depression caused by surfactant accumulation at moving gas–liquid interfaces. In order to define and justify the domain of validity of the dimensionless results, which represent the effect of gas transfer depression, we describe in this paragraph the theoretical modelling of the surfactant interfacial accumulation, which is the cause.

3.1. Transient surface accumulation

Bubble formation begins with the previous bubble detaching and causing a singularity in the physical system. In the precise instant of bubble detachment the gas–liquid interface at the orifice is exposed to a contamination equal to the liquid bulk, which has much smaller magnitude than the surface contamination of the just detached bubble, and may be considered negligible. In the transient time between detachments of two bubbles a time-dependent contamination occurs at the gas–liquid interface. The parameter that quantifies surface accumulation is $\Gamma(t)$ $(mol\,m^{-2})$, which in atmospheric aqueous solutions is a function of temperature, surfactant nature, and surfactant bulk concentration. This is recorded in our experiments as a variation of dynamic surface tension.

The time-dependent diffusion-controlled dynamic interfacial adsorption kinetics at air-aqueous surfactant solutions was first quantified with an analytical equation by Ward and Tordai (1946). Their equation relates surfactant interfacial accumulation $\Gamma(t)$ with surfactant interfacial concentration and diffusivity for planar surfaces, accounting for surfactant back-movement to the subsurface (in the integral term). The subsurface is defined as the surface of the spherical region outside the semi-spherical forming bubble with diameter equal to the capillary. Following the procedure by Liu et al. (2004), which is reported in detail in Appendix A, the diffusion equation

$$\frac{\partial c(r,t)}{\partial t} = D_{\mathrm{SAA}} \nabla^2 c \tag{3}$$

can be combined with Fick's first law

$$\left.\frac{\partial \Gamma(t)}{\partial t}\right|_{r_0} = \left.\frac{\mathrm{d}\Gamma(t)}{\mathrm{d}t}\right|_{r_0} = D_{\mathrm{SAA}} \left.\frac{\partial c(r,t)}{\partial r}\right|_{r_0} \tag{4}$$

and solved at the gas–liquid interface for short-time limits as

$$\Gamma(t) = \frac{D_{\mathrm{SAA}} \cdot c_B \cdot t}{r_0} + 2c_B \left(\frac{D_{\mathrm{SAA}} \cdot t}{\pi}\right)^{1/2}, \tag{5}$$

Eq. (5) is the short-time solution to the Ward–Tordai equation and relates surface accumulation $\Gamma(t)$ with time, bulk concentration, and orifice diameter. Note that Eq. (5) is a continuously growing function, hence does not describe surface saturation occurring at long-time limits.

3.2. Equilibrium surface accumulation

For diffusion-controlled adsorption a Langmuir isotherm is suitable to relate dynamic surface tension $\gamma(t)(N\,m^{-1})$, equilibrium surface tension $\gamma_\infty(N\,m^{-1})$, and dynamic interfacial adsorption (or surface accumulation) $\Gamma(t)(mol\,m^{-2})$:

$$\gamma(t) = \gamma_\infty + RT \cdot \Gamma_\infty \cdot \ln\left(1 - \frac{\Gamma(t)}{\Gamma_\infty}\right), \tag{6}$$

where Γ_∞ is the limiting surface accumulation at equilibrium $(mol\,m^{-2})$, R the universal gas constant $(J\,mol^{-1}\,K^{-1})$ and T the absolute temperature (K). Expanding the logarithm in Eq. (6) into a series and truncating after the first term we obtain the approximation of Eq. (6) for quasi steady-state conditions:

$$\gamma(t) = \gamma_\infty - RT \cdot \Gamma(t), \tag{7}$$

Eq. (7) can be solved for $\Gamma(t)$, when γ_0 and $\gamma(t)$ are known:

$$\Gamma(t) = \frac{\gamma_\infty - \gamma(t)}{RT}. \tag{8}$$

The dynamic interfacial accumulation $\Gamma(t)$ approaches the equilibrium value Γ_∞ at very long bubble age limit. This occurs in the long time limit because surface contaminants concentration has reached a constant value. This also causes the dynamic surface tension to approach a minimum, constant value.

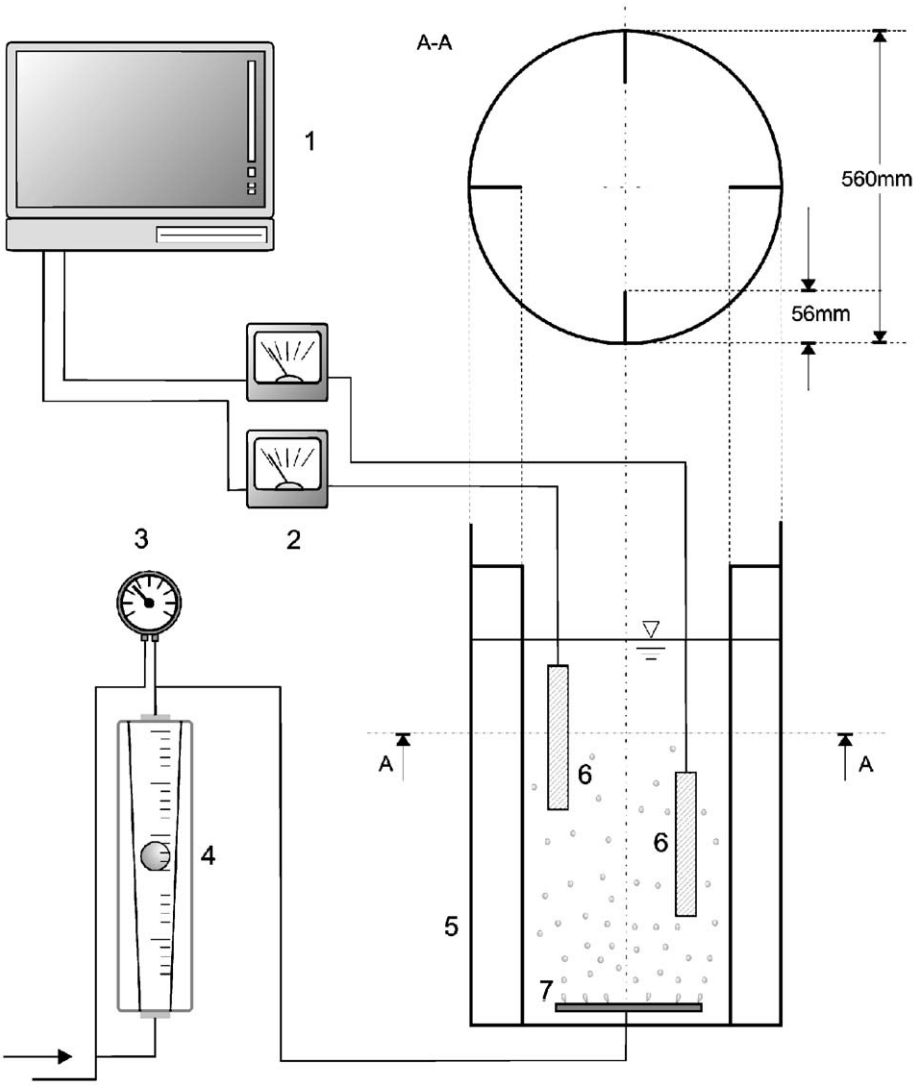

Fig. 3. Aeration apparatus: computer for signal logging (1), dissolved O_2 meters (2), differential pressure gauge (3), rotameter (4), aeration vessel (5), dissolved O_2 probes (6), fine-pore diffuser (7).

The equilibrium surface accumulation can be extrapolated from $\Gamma(t)$ patterns at long-time limits, as well as calculated from the Gibbs equation (for a surfactant solution of concentration c_B)

$$\Gamma_\infty = -\frac{1}{RT}\frac{\mathrm{d}\gamma_\infty}{\mathrm{d}\ln c_B}, \tag{9}$$

which treats adsorption as a thermodynamic process. The ratio $\mathrm{d}\gamma_\infty/\mathrm{d}\ln c_B$ can be calculated from the slope of the semi-logarithmic surfactant characteristic curve (Fainerman et al., 1994), such as the curve represented in Fig. 4, which relates equilibrium surface tension to the surfactant bulk concentration.

3.3. Model comparison and domain

The surface accumulation was calculated with both Eqs. (4) and (8), i.e. by using both the Langmuir and the Ward–Tordai adsorption models, respectively. Fig. 5 shows a comparison of the two results. The Ward–Tordai method gives a time-dependent solution derived from diffusivity, time, and geometrical parameters, while the Langmuir approach derives phenomenologically the surface accumulation directly from its effect, i.e. the dynamic surface tension change. At short-time limits, the Langmuir equation overestimates the results of the Ward–Tordai equation, but is within the same order of magnitude. At long-time limits, the Ward–Tordai short-limit approximation overestimates surface accumulation, as it does not account for saturation of interfacial adsorption sites and back-diffusion (the subsurface concentration term in Eq. (5)). The point where the two models predict the same result represents the inception of the steady-state regime. Hansen (1960) showed that his long-time limit solution of the Ward–Tordai equation agrees with the Langmuir equation (Eq. (9)) within 1% of error when $\Gamma(t_B)/\Gamma_\infty > 0.7$.

In all our data sets, the bubble detachment time is always within the domain of the Langmuir model. This is equivalent to say that when bubbles detach with these air flowrates the surface contamination already reached equilibrium, i.e. the surfactant activity is at steady-state. In the following sections this

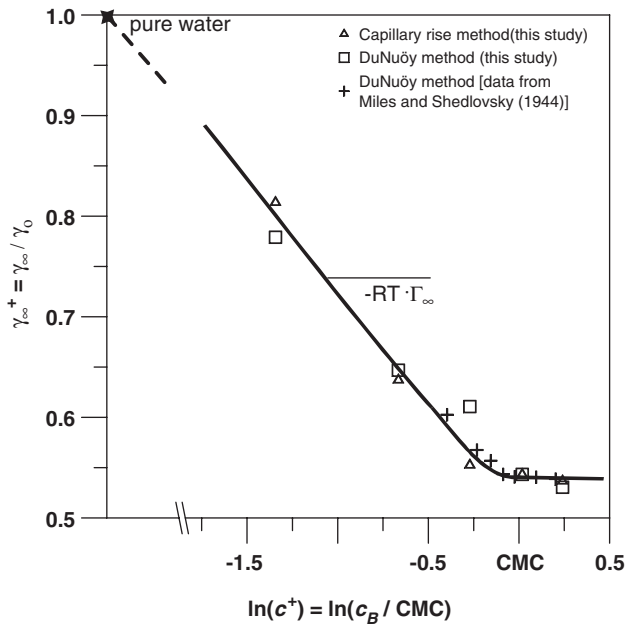

Fig. 4. Dimensionless characteristic curve for sodium dodecyl sulphate solutions. The horizontal axis is the natural logarithm of the dimensionless concentration $c^+ = c_B/\mathrm{CMC}$, where CMC is the critical micelle concentration. The vertical axis is the dimensionless equilibrium surface tension, i.e. the equilibrium surface tension divided by the solvent surface tension. At null c^+ values, the surface tension is the equilibrium surface tension of pure water. Data points labelled "+" are DuNuÖy measurements from Miles and Shedlovsky (1944).

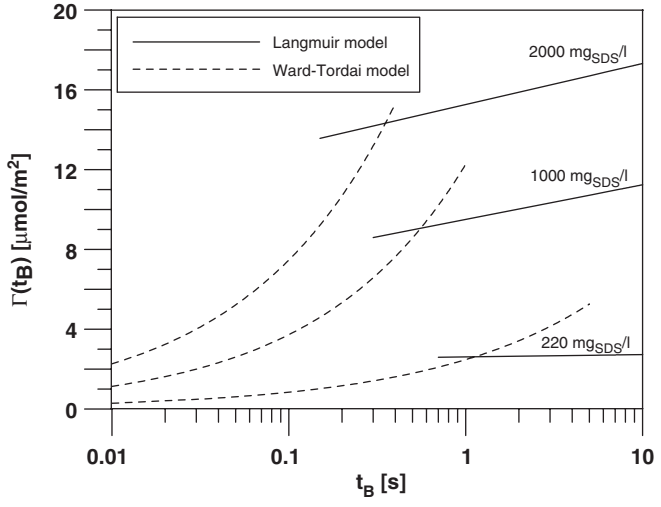

Fig. 5. Interfacial surfactant accumulation $\Gamma(t_B)$ described by the Ward–Tordai and Langmuir models. The Ward–Tordai model well describes the net migration towards the surface occurring at short-time limits, while at long-time limits the Langmuir model shows the establishment of dynamic equilibrium at the interface.

theoretical discussion is confirmed by results that describe the bubble flow regime to fit the solid-sphere model, consequence of the equilibrated surface contamination, as described by the Langmuir model.

4. Results and discussion

Equilibrium surface tension measurements were performed, with results presented in dimensionless form in Fig. 4. SDS Concentrations were normalized to the CMC value available in literature of 2360 mg l^{-1} (Rosen, 1978). Thus, by defining the reduced concentration c^+ as the surfactant concentration over the CMC, $\ln(c^+)$ will be equal to 0 at the CMC. In the same way, the measured value of the static surface tension of pure water ($c^+ = 0$) was used to normalize the vertical axis. At zero contamination ($\ln(c^+) \to -\infty$), the surface tension is same as pure water ($\gamma^+ = 1$). Surface tension values decrease rapidly starting with low contamination. In the case of pure water, H_2O molecules are organized at the interface in a lattice which is in a dynamic equilibrium state (i.e., the interfacial layer is continuously renewed, and each molecule experiences the hydrogen bond interaction of its neighbouring fellow molecules). At zero contamination, the distribution of tensile stresses on the interface is uniform and its statistical sum is zero, hence the spherical shape of the bubble. When contamination is present, the lattice made of water molecules is divided in sub-lattices that are separated by surfactant molecules. Due to the partially hydrophobic nature of surface active agents, hydrogen bonds between surfactants and sub-lattices will not establish, and each sub-lattice will not experience the hydrogen interaction of neighbouring ones because of their distance forced by surfactant molecules. The overall effect is a lower force required to separate sub-lattices from each other, and an observable decrease in surface tension. A higher number of accumulated surfactant molecules will result in smaller sub-lattices, therefore lower surface tension for higher contaminations.

Fig. 6 shows the concurrent measurement of DST and k_La for a 50 mg l^{-1} SDS solution for a single-bubble at low

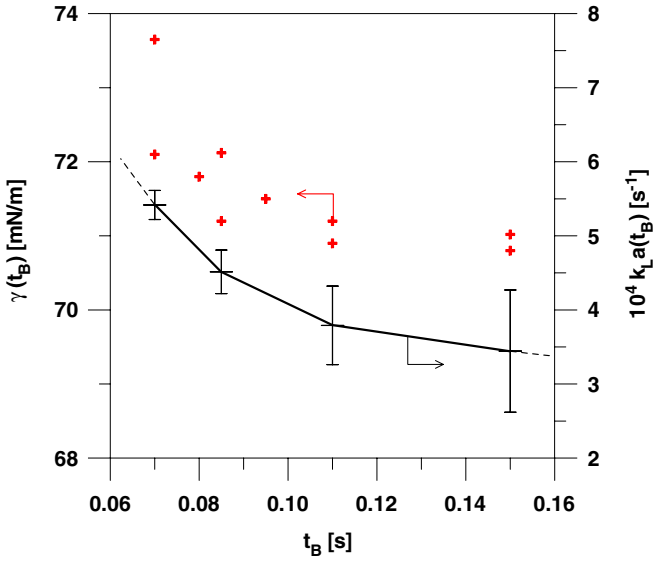

Fig. 6. Dynamic surface tension and volumetric mass transfer coefficient for 50 $\mathrm{mg_{SDS}}/l$ solutions. Both parameters decrease with increasing time. Bars represent one standard deviation. Note that a modest variation in $\gamma(\sim 3\%)$ may reflect a large variation in k_La ($\sim 30\%$).

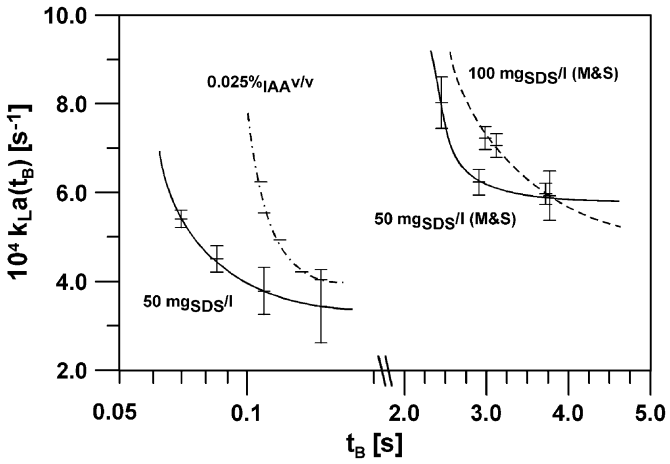

Fig. 7. Mass transfer coefficient evolution with time. The time-scale is logarithmic for the short-time limit and linear for the long-time limit. Data is from both this study (H) and previous investigations in our laboratory (Masutani and Stenstrom, 1991; labelled "M & S"). Bars represent one standard deviation of data points (IAA not visible because single-trial).

interfacial speed ($u \sim 10^{-2}\,\mathrm{m\,s^{-1}}$). It is clear the direct correlation between the two trends. As time progresses, the interfacial accumulation increases and rapidly reaches a steady value. In fact, for $t_B > 0.12\,\mathrm{s}$ the DST reaches a stationary value. In Fig. 6 the solid line connects the average k_La values, and vertical error bars represent one standard deviation. The mass transfer coefficient is maximum at bubble formation, and rapidly decreases with DST. The initial k_La value corresponds to the value in pure water, and the final k_La value (at bubble detachment) is about 40–70% of the initial one. In field engineering practice, this is reflected in overall O_2 process transfer rates about 40–70% the transfer rates in pure water. It is interesting to note that a modest decrease in DST ($\sim 3\%$) corresponds to a considerable decrease in k_La ($\sim 35\%$).

Fig. 7 shows results from multi-bubble mass transfer coefficient measurements of SDS solutions in a controlled temperature environment ($\pm 0.3\,^{\circ}\mathrm{C}$). As shown in Fig. 6, DST declines with analogous pattern as k_La, and is not plotted in Fig. 7 for clarity. For clarity, the vertical axes are in log scale and the horizontal axis has a log scale for $t_B < 0.25\,\mathrm{s}$. Solutions with higher SDS concentrations have higher slopes due to higher surfactant interfacial accumulation. At very long-time limits, all slopes will reach plateaus. At the initial time range, the surface tension remains at approximately the value of pure water, and starts to decrease only after a lag time. Higher concentrations will show a shorter lag-time and a lower equilibrium surface tension, due to larger quantities of contaminants accumulating on the bubble surface over time. The existence of lag behaviour is due to the fact that concentrations in Fig. 7 are below CMC. Therefore, there is no excess of surfactant in the solution and the surfactant employs a finite time to contaminate the surface. As the concentration approaches CMC, the lag time reduces in length, and when the concentration is above CMC there exists a surfactant excess in the solution, and the surface contamination effect is immediate, i.e. without lag. Several tests reported in literature show no lag time for surfactant concentrations above CMC (Datwani and Stebe, 2001; Daniel and Berg, 2003). Also, concentrations higher than the CMC will show a dynamic surface tension pattern converging to the same plateau, as the equilibrium surface tension above CMC does not vary (Fig. 4).

Fig. 7 shows values of the volumetric liquid-side mass transfer coefficient k_La. Several runs were performed for each elapsed time, and bars represent one standard deviation. The volumetric mass transfer coefficient is calculated from dissolved oxygen concentration values using Eq. (1). It is evident from the graph that mass transfer coefficients decline very rapidly with increasing time. The first observation about k_La is that IAA causes a more rapid decline in mass transfer, but after a longer lag time. This is likely due to the presence of a OH-functional group in the IAA molecule, which, combined with its lower molecular weight than SDS, hence a higher affinity to water molecules than SDS (the carbon tail is the hydrophobic component for both molecules), results in lower exclusion forces that are the driving force of interfacial accumulation. IAA diffusivity ($\sim 10^{-9}\,\mathrm{m^2\,s^{-1}}$@$25\,^{\circ}\mathrm{C}$) is lower than SDS diffusivity ($\sim 10^{-10}\,\mathrm{m^2\,s^{-1}}$@$25\,^{\circ}\mathrm{C}$), and, in general, because of this property, surfactants with higher migration velocity are usually referred to as fast surfactants (Ferri and Stebe, 2000). Conversely, surfactants with lower migration velocity are usually named slow surfactants. Nevertheless, the establishment of hydrogen bonds between water and IAA retards its surface contamination effects, measurable as decline of DST and k_La.

Surfactant migration velocity is dependent on the chemical nature of the surfactant. In general, when approximating non-interacting surfactants molecules to spheres, higher molecular weight surfactants have lower migration velocities. However, care is necessary when considering macromolecules and poly-charged compounds that are likely to adopt steric configurations not assimilable to a spherical shape. Also, dissociated species such as salts or alcohols may behave as gas transfer enhancers, and their solutions may show apparent gas transfer coefficients several fold the gas transfer coefficient of pure water (Zlokarnik, 1980). Yet, this effect is compensated by a much larger decline of the O_2 saturation concentration in these solutions, with a net result of decreased overall gas transfer.

Different flow regimes have different mass transfer coefficients, and it is necessary to limit the comparison between contaminant concentrations to the same flow regime. In Fig. 7, mass transfer coefficient measurements for SDS solutions previously recorded (Masutani and Stenstrom, 1991) have higher values than the coefficients measured in this study. This occurs because the current flow regime is lower than the flow regime previously adopted. Nonetheless, data patterns for $50\,\mathrm{mg_{SDS}\,l^{-1}}$ appear similar but shifted on the graph. Higher flow regimes result in higher interfacial renewal rates, hence in a retardation of the surface contamination effects. Moreover, the equilibrium value of the mass transfer coefficient will be higher for higher flow regimes, as mass transfer is also proportional to interfacial velocity. In the data by Masutani and Stenstrom (1991) the patterns for 50 and $100\,\mathrm{mg_{SDS}\,l^{-1}}$ intersect at longer-time limits (at $t_B \sim 4\,\mathrm{s}$). After intersecting, the mass transfer

behaviour for higher SDS concentration reaches a lower equilibrium value, since both experiments (at 50 and 100 $mg_{SDS}\,l^{-1}$) were conducted at the same flow regime, hence at the same surface renewal rate, and higher mass transfer depression occurs at higher contaminant concentration. Still, interfaces with higher renewal rates have a comparable decline for different contaminations (50 and 100 $mg\,l^{-1}$) than interfaces with same contamination (50 $mg\,l^{-1}$) and different flow regimes [$\log(Pe)_s \sim 6$ and 8]. By comparing the magnitude of contamination and flow regime effects, we can conclude that higher flow regimes can offset the effects of contamination.

5. Dimensional analysis of results

In order to generalize the results and compare different flow regimes, geometries and contaminations, a dimensional analysis was performed. The method used is based on the Buckingham-Pi theorem, and the procedure is by Zlokarnik (2002). The physical quantities included in the analysis were: bubble life t_B, mass transfer coefficient $k_La(t_B)$, bubble diameter $d_B(t_B)$, orifice diameter d_0, dynamic surface tension $\gamma(t_B)$, weight (i.e., buoyancy) of the bubble $g\Delta\rho$, bulk surfactant concentration c_B, surfactant bulk diffusivity D_{SAA}, airflow rate Q, and oxygen interfacial diffusivity $D_{s,\mathrm{O}_2}(t_B)$. Due to the low shear rate of this process, the liquid viscosity has no influence and is thereby excluded from the analysis. Highly viscous systems need a different dimensional analysis, because the transport phenomena occurring in those systems are due to different transport mechanisms.

The oxygen interfacial diffusivity was calculated by solving Higbie's formula (1935):

$$k_{L,\text{clean water}} = 1.13\sqrt{u_B \cdot D_{s,\mathrm{O}_2}/d_B} \tag{10}$$

for D_{s,O_2}. This diffusivity was chosen in lieu of the oxygen bulk diffusivity to scale for flow effects and include in the dimensional analysis the effective diffusivity that a moving interface experiences. However, this diffusivity does not account for contamination, since the domain of Eq. (10) is pure gas–liquid systems. Therefore, the oxygen diffusivity that is included in this dimensional analysis is that of a bubble moving with its measured velocity in pure water. The introduction of an oxygen interfacial diffusivity results in the definition of interfacial dimensionless numbers, in analogous fashion as reported in Sadhal et al. (1997).

The surfactant bulk diffusivity is used in the analysis and the effects on the interface are reflected to the gas-side by including the time-dependent dynamic surface tension. The use of a surfactant time-dependent diffusivity in the analysis may result in redundancy and in problems with statistical significance, as the time-dependent interfacial surfactant diffusivity is calculated as a function of the dynamic surface tension itself. The liquid-side interfacial diffusivity was calculated solving the Ward–Tordai model to corroborate the results of the dimensional analysis (Rosso, 2005). This confirmed the expectations that gas and liquid side interfacial diffusivities concurrently change with increasing time (Ferri and Stebe, 2000).

Frössling (1938) performed a dimensional analysis on bubble gas transfer systems that lead to the well-known empirical formula:

$$(Sh) = a \cdot (Re)^b \cdot (Sc)^c \tag{11}$$

where (Sh), (Re), and (Sc) are the Sherwood, Reynolds, and Schmidt numbers, respectively; a, b, and c are empirical fitting parameters. Table 1 includes the extended notation for these dimensionless numbers, and their physical significance. The bubble–droplet duality allows the use of Eq. (11) for droplets as well. The Frössling empirical equation relates gas transfer to the flow regime, with higher mass transfer for higher bubble velocities. At no flow, Eq. (11) predicts zero mass transfer. This means that the mass transfer condition at stagnation, i.e. $(Sh) = 2$, is neglected in this formulation.

There are numerous observations in literature for the fitting parameters a, b, and c (e.g.: Levich, 1962; Acrivos and Goddard, 1965; Lamont and Scott, 1970). Depending on the process conditions, there exist correlations between the model limits of rigid and circulating spheres (Clift et al., 1978). Since $(Re) \cdot (Sc) = (Pe)$, Eq. (11) may be rewritten as (Lamont and Scott, 1970):

$$(Sh) = a' \cdot (Pe)^{b'} \tag{12}$$

where a' and b' are empirical constants. The exponent b' is reported to range between 1/3 for solid surfaces to 1/2 for circulating surfaces (Levich, 1962; Acrivos and Goddard, 1965; Lamont and Scott, 1970; Clift et al., 1978). Eq. (12) shows the analogy between mass diffusivity (i.e., the mass transfer coefficient k_La) and advective forces (the bubble velocity u).

A dimensional analysis on our data sets lead to the dimensionless numbers reported in Table 1. Π_1, $(\Pi_2)^{-1}$, and Π_6 are the interfacial Sherwood, Bond, and Péclet numbers $[(Sh)_s, (Bd)_s, (Pe)_s]$, respectively. Π_3 and Π_5 are named the dimensionless characteristic length d^+ and time t^+, for sake of clarity. Π_4 is named the gravitational contamination number (Sm). For our data sets, (Bd) varies between 0.9 and 0.1, confirming that for our experiments surface tension has a dominant effect on gravity forces. (Sm) represents the ratio of diffusion from bulk towards the interface to gravity forces, and has values in the order of 10^{-18} for all measurements in our data sets. This means that gravity has a much larger weight than diffusional forces in our experiments. Nevertheless, small diffusional forces (i.e., the cause) can result in severe variations of interfacial tension (i.e., the effect). By defining the surface contamination number:

$$(Ro) = \frac{(Sm)}{(Bd)} \cdot (D^+)^2 \cdot t^+ = \frac{c_B \cdot t_B \cdot D_{B,\mathrm{SAA}}^3}{\gamma \cdot d_B^3} \tag{13}$$

which quantifies the ratio of surface contamination to surface tension forces, the system can be defined by the pi-set:

$$(Sh)_s = f\{(Pe)_s, (Bd), (Sm), t^+, d^+, D^+\} \simeq f\{(Pe)_s, (Ro)\}. \tag{14}$$

The dimensionless length-scale d^+ was contained within a narrow range throughout our data set, and showed no improve-

Table 1
Dimensionless numbers, notation, and their physical significance

Symbol	Pi-notation	Extended notation	Physical significance
$(Sh)_s$	Π_1	$\frac{k_L a \cdot d_B^2}{D_{s,O_2}}$	$\frac{\text{Mass diffusivity}}{\text{Molecular diffusivity}}$
(Bd)	$(\Pi_2)^{-1}$	$\frac{g\Delta\rho \cdot d_B^2}{\gamma}$	$\frac{\text{Gravity force}}{\text{Surface tension}}$
d^+	Π_3	$\frac{d_0}{d_B}$	Dimensionless length-scale
(Sm)	Π_4	$\frac{c_B \cdot D_{s,O_2}^2}{g\Delta\rho \cdot d_B^3}$	$\frac{\text{Surface contamination}}{\text{Gravity force}}$
t^+	Π_5	$\frac{t_B \cdot D_{s,O_2}}{d_B^2}$	$\frac{\text{Geometrical time scale}}{\text{Diffusional time scale}}$
D^+	Π_6	$\frac{D_{SAA}}{D_{s,O_2}}$	Dimensionless diffusivity
$(Pe)_s$	Π_7	$\frac{Q}{d_B \cdot D_{s,O_2}}, \frac{u \cdot d_B}{D_{s,O_2}}$	$\frac{\text{Advective forces}}{\text{Diffusive forces}}$
(Ro)	$\Pi_2 \cdot \Pi_4 \cdot \Pi_6^2 \cdot \Pi_5$	$\frac{c_B \cdot t_B \cdot D_{SAA}^3}{\gamma \cdot d_B^3}$	$\frac{\text{Surface contamination (}cause\text{)}}{\text{Surface tension (}effect\text{)}}$
(Re)	—	$\frac{d_B \cdot u}{\nu}$	$\frac{\text{Inertial forces}}{\text{Viscous forces}}$

$(Sh)_s$ and $(Pe)_s$ are the interfacial Sherwood and Péclet numbers. (Bd) is the Bond number and (Sm) is defined as the gravitational contamination number. The last two dimensionless numbers (Ro) and the Reynolds number (Re) are not a direct result of the dimensional analysis.

ment of the regression analysis. We analyzed the bubble size distribution for each surfactant and compared it to the Sauter diameter (the sum of the diameters cubed divided by the sum of the diameters squared). For all data sets the Sauter diameter was very close to the mean bubble diameter, showing that the bubble size distribution was normal with low variance. The bubble rise velocities showed a similar low variance.

Nonlinear regression analyses were performed using SYSTAT 10 (SPSS Corporation, Chicago, IL). The data were fit using the following equation:

$$(Sh)_s = \frac{0.382 \cdot (Pe)_s^{1/3}}{1 + \log[1 + 10^{19} \cdot (Ro)]} \tag{15}$$

which is statistically significant ($R^2 > 0.8$; $t > 10$; $P < 10^{-3}$; unbiased residuals). The numerator of Eq. (15) is an interfacial version of the well-known Frössling equation. Eq. (15) relates mass diffusivity $(Sh)_s$, advective forces $(Pe)_s$, and contamination effects (Ro) at the gas–liquid interface. At zero flow, Eq. (15) reads no mass transfer.

In order to present the evolution of mass transfer with increasing time in a dimensionless form, $(Sh)_s$ was plotted versus the dimensionless time (Fig. 8). In this log–log plot, the trendlines are linearized and labels represent $\log(Pe)_s$ for selected points. Note that $(Pe)_s$ is the interfacial Péclet number, calculated using the interfacial O_2 diffusivity (which is reduced when compared to O_2 bulk diffusivity). As a consequence, $(Pe)_s$ values in this paper appear higher than (Pe) calculated using bulk diffusivity. Nevertheless, the relative ratio between $(Pe)_s$ characterizing experiments with different flow regimes and surfactants remains unchanged. Four main results are evident: (1) $(Sh)_s$ declines over time, (2) the slope of the trendlines are dictated by the contamination [type of contaminant and concentration, quantified by (Ro)], (3) intercepts are a function of flow regime and contamination, and (4) intercepts, at a given contamination, are dictated by the flow regime $[(Pe)_s]$ only.

The slight decline of $(Pe)_s$ is due to the increase in interfacial drag due to contamination. The oxygen interfacial diffusivity decreases rapidly at the initial phase of contamination, but this effect does not increase $(Pe)_s$ (the diffusivity is at the denominator, as in Table 1), because both interfacial velocity and bubble diameter appear in the numerator, and are both depressed with contamination. The overall effect is a slight decline of $(Pe)_s$, observable as a slightly lower bubble terminal rise velocity after detachment, for all the cases presented, if compared to pure water tests.

SDS data from this study have the same slope as SDS data from our previous investigations, while its position is shifted to the bottom of the plot, due to lower initial Péclet numbers. The slope of the IAA data fit is slightly higher than the slope of SDS data fits, due to higher migration velocity towards the interface for IAA. Also, the intercept of the IAA trendline is higher, at comparable interfacial velocity, confirming the retardation in DST depression by IAA molecules, when compared to SDS. TGT (sodium *n*-tetradecyl sulphate, F.W. = 316.44, CAS No. 1191-50-0) data from our previous investigation are also included in Fig. 8. This higher molecular weight surfactant shows a slower decline in mass transfer, a consequence of its lower migration velocity. The TGT points cluster around six parallel lines, which are parametric in (Ro). The lines are nearly parallel but will begin to converge at longer time limits, since the bubble diameter, included in definition of (Ro), is reduced by surfactant bulk concentration. From the top of the graph, the surfactant bulk concentration increases from 0.07 CMC to 0.45 CMC. The intercepts vary according to the initial

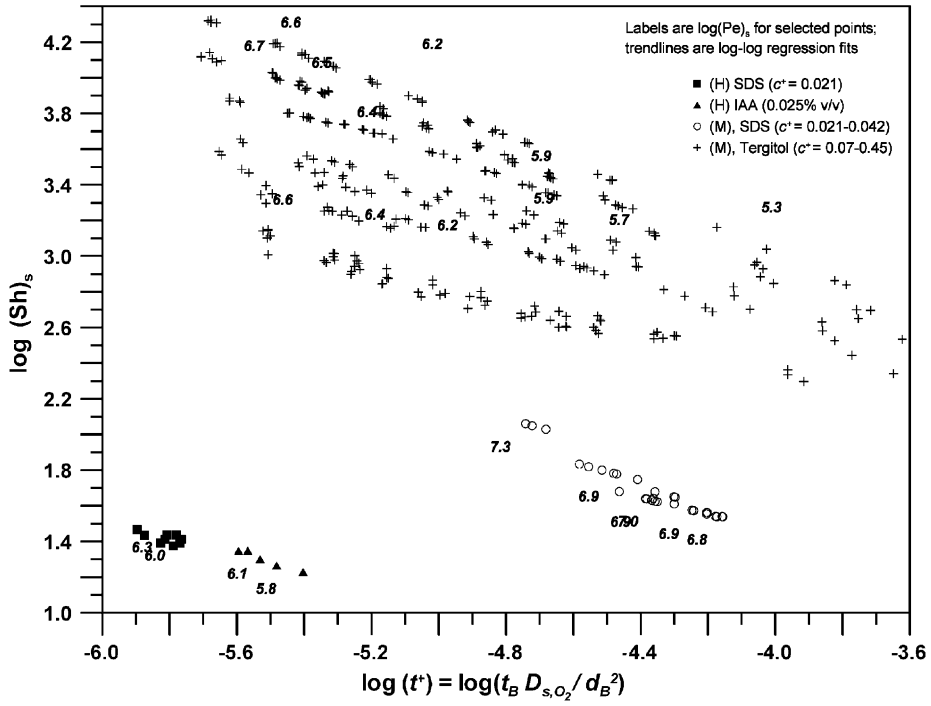

Fig. 8. Dimensionless representation of mass transfer phenomena with time. $(Sh)_s$ is the interfacial Sherwood number and t^+ is the dimensionless time-scale (see Table 1 for definitions). The surfactants included in this plot are sodium dodecyl sulphate, iso-amyl alcohol, and sodium tetradecyl sulphate (TGT). Labels are $\log(Pe)_s$ for selected points. Solid lines are log–log regression fits.

contamination. This is in accord with observation 3), stated previously, where for a given contamination the intercept is a sole function of $(Pe)_s$ at a given contamination, but higher contamination results in lower intercepts.

Fig. 9 shows the evolution of interfacial mass transfer in dimensionless form during a time-dependent case. The interfacial Sherwood number (representing mass transfer) declines very rapidly over time, a consequence of a slight decline in $(Pe)_s$ (representing advection) and a rapid growth in surface contamination (Ro). As the interface starts forming, surfactants rapidly migrate towards it, driven by van der Waals exclusion forces. This results in interfacial gas diffusivity smaller than bulk diffusivity. Although the interfacial gas diffusivity appears at the denominator in $(Sh)_s$, its effect on the equation does not bias the result, as it is present in the denominator of $(Pe)_s$ as well. The value of γ is known to decline with increasing time, which is accounted in the denominator of (Ro). Thus, with increasing time, Eq. (15) shows the analogy between increasing interfacial contamination effects (measured via the dynamic surface tension decline) and the depression of mass transfer. In their classical form, Eqs. (11) or (12) would show the proportionality of mass transfer to advective forces, but would not quantify the evolution of mass transfer decline and interfacial contamination increase (i.e., surface tension decline) over time. Our model predicts mass transfer more accurately for $(Sh)_s < 10^2$. Mass transfer above this threshold can be achieved by gas–liquid interfaces moving fast enough to belong to the fluid sphere domain. This is the domain of coarse bubbles in process water or possibly of fine-bubbles in pure water.

Fig. 9 reports also a form of the Frössling equation form Clift et al. (1978). This equation fits the data well at very short-time limits beyond the range of our data sets, where the contamination still has negligible effect. This is characteristic of the inception of bubble formation, or of interfaces moving with such a velocity to have no significant interfacial accumulation. All data in our data sets and all fine-bubbles moving in water solutions in the gravitational field do not belong to this domain. The Frössling equation predicts mass transfer well for fine-bubbles in pure water or for contaminated solutions beyond current practical applications.

Finally, Fig. 10 shows the limit of applicability of Eq. (15) in terms of flow regime. The horizontal axis reports $(Pe)_s$ and the vertical axis $(Sh)_s$. The family of parallel trendlines is parametric in (Ro). Higher contamination, hence higher (Ro), results in a trendline shift downwards in the graph. When contamination effects are dominant [$(Pe)_s < 10^7$], Eq. (15) describes the experimental data with its exponent for (Pe) of 1/3, which characterizes the solid sphere approximation. For higher interfacial velocities or coarser bubbles, contamination is offset by higher interfacial renewal rates. This is domain for bubbles behaving as fluid spheres. Hence, the exponent for (Pe) in this region approaches 1/2. In Fig. 10 it is possible to see that at $(Pe)_s \sim 10^7$ the data points start transitioning from solid- to fluid- sphere regimes. For both regimes, the pure water case, fitted with a Frössling equation, represents the upper limit for oxygen transfer. The comparison with pure water tests show that contamination as high as $(Ro) \sim 10^{-19}$ can be offset by high flow regime: in Fig. 10 the trendline for pure water points

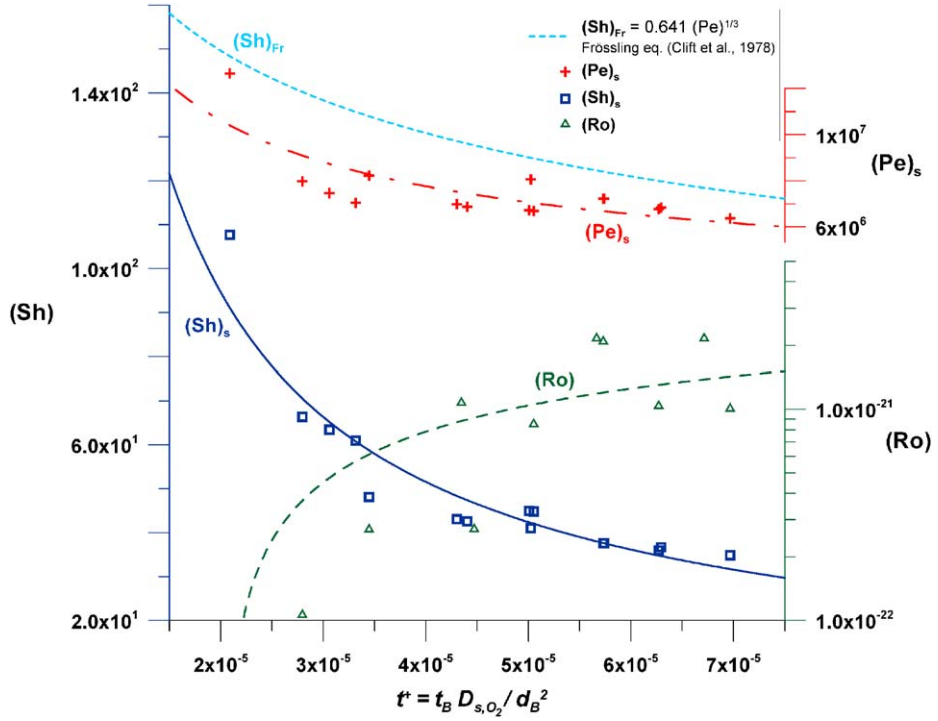

Fig. 9. Dimensionless representation of mass transfer and contamination phenomena with time for a selected time-dependent experiment. $(Sh)_S$, $(Pe)_S$, and (Ro) are the interfacial Sherwood, the Péclet, and the second contamination numbers, respectively; t^+ is the dimensionless time-scale (see Table 1 for definitions); $(Sh)_{Fr}$ is the Sherwood number calculated with the Frössling equation (from Clift et al., 1978).

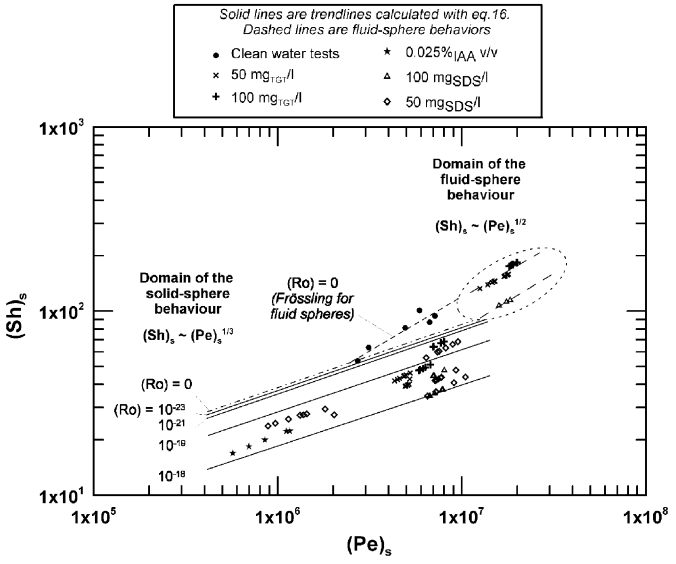

Fig. 10. Dimensionless representation of mass transfer $(Sh)_S$ as a function of flow regime $(Pe)_S$ and of contamination (Ro). The domain of Eq. (16) is $(Pe)_S < 10^7$, and at $(Pe)_S \sim 10^7$ the transition between solid- and fluid-sphere behaviour commences. The Frössling equation represents the upper limit for mass transfer, i.e. fluid-spheres in pure liquid. This limit is approached at low interfacial velocity with very low contamination $[(Ro) \to 0]$ or with increasing interfacial velocity $[(Pe)_S > 10^7]$. The higher the $(Pe)_S$, the lower the weight of contamination on gas transfer.

(fluid sphere approximation, fitted with a Frössling equation) is very close to the trendline for contaminated solutions, showing the expected behavior for coarser bubbles, i.e. reduced gas transfer depression. This region corresponds to economically disadvantageous, if not unfeasible, operations in fine-bubble aeration in the gravitational field.

6. Recommendations for scale-up

Aeration systems for biological environmental processes are traditionally designed relying upon data collected from re-aeration tests in pure water. The scale-up factors are commonly left to the designer's experience. However, this has resulted in frequent overestimation of performance. Pure water re-aeration tests are characterized by bubbles belonging to the fluid-sphere regime, while process water tests can be characterized by both the fluid- and solid-sphere regimes. Bubble diameter, gas flowrate, and contaminant quantitative and qualitative characteristics determine the transition between the two regimes.

In our experimental setup full scale conditions were produced for a single bubble. The bubble characteristics (diameter, velocity, time scale) and surfactant concentrations are in the same range as in full scale. The difference between laboratory and full scale is only the number of bubbles. Our aeration experiment, as shown in Fig. 3 was performed using a full-scale diffuser and confirms that the similitude between the laboratory- and full-scale system is maintained.

Fig. 9 shows the celerity of gas transfer depression operated by SDS. In Fig. 9 the departure between the two solutions begins at bubble formation and reaches a steady value before bubble detachment. In aerated biological processes such as

sequencing batch reactors, PFR, or CSTR reactors, the average hydraulic retention time for a fine-bubble is in the order of 20–80 s. This reduces the time of bubble formation to a negligible fraction of the total bubble residence time. Therefore, the gas transferred in the bubble formation process is a negligible fraction of the total gas transferred.

When sizing aeration systems for contaminated liquids it is necessary to take the corrected $k_L a$ value that can be calculated from Eq. (15), and not the Frössling solution. Design engineers typically utilize

$$\alpha = \frac{k_L a_{\text{process water}}}{k_L a_{\text{pure water}}} \tag{16}$$

as a scaling factor to account for process conditions. In unusual cases, when greater than one, such as in certain inorganic salts and aliphatic alcohols (Zlokarnik, 1980), alpha has been called an enhancement factor, m. Our results can be expressed in terms of alpha:

$$\alpha \sim \frac{(Pe)_s^{2/3}}{1 + \log[1 + 10^{19} \cdot (Ro)]} \tag{17}$$

Eq. (17) is the ratio of Eq. (15) and the interfacial Frössling form of Eq. (12). Note that the flow effects do not cancel, as in our flow regime the bubbles behave as solid spheres but the Frössling prediction is for fluid spheres. For fine-pore aerators, alpha factors typically range from 0.2 to 0.8, depending on the contaminant characteristics. This implies a design over sizing of 1.25–5 times the aeration capacity in pure water. The choice of alpha factors for biological process design is crucial for overall efficiency and economic viability of the aeration process (Rosso et al., 2005).

7. Summary and conclusions

Commercially available surfactants were used to concurrently measure dynamic surface tension and mass transfer coefficients. Measurements were performed from bubble formation to bubble detachment, showing that for fine-bubbles in aqueous surfactant solutions, surface contamination equilibrates before detachment. Therefore, after bubble detachment and during the transit of bubbles through the liquid, the liquid-side gas transfer coefficient is reduced to a steady-state process value, always lower than the gas transfer coefficient in pure water. Our experimental evidence shows a reduction of 30–70% of pure water values in surfactant solutions, which confirms full-scale field measurements.

By accumulating at the interface, surfactants lower the surface tension, reduce interfacial renewal, and reduce the diffusion of gas into the liquid. For a given contamination, interfaces with higher renewal rates have higher mass transfer. For a given flow regime, hence a given renewal rate, higher contamination results in lower mass transfer. At higher renewal rates, the variation due to different contamination is smaller than the variation at lower renewal rates. We conclude that higher flow regimes can offset contamination.

Bubble flow regime can be described by the solid-sphere approximation for fine-bubbles in surfactant solutions, or by the fluid-sphere approximation for coarse bubbles or for fine-bubbles in pure water. This is reflected in a different relationship between the Sherwood and Péclet numbers, with exponent for (Pe) ranging from 1/2 to 1/3 for fluid- and solid-spheres, respectively.

Dynamic surface tension decline has a direct correlation to mass transfer coefficient decline for all cases presented, and it is used to correct the empirical equations for gas transfer in pure liquids. In the case of surfactant solutions, empirical correlations in the form of the Frössling equation are scaled to lower, measurable values with the introduction of a surface contamination number (Ro) at the denominator. This dimensionless number describes the ratio of surface contamination causes to surface contamination effects, by including parameters for both quantity and quality of contaminants. Our dimensional analysis results in correlations that quantify the evolution of mass transfer decline and interfacial contamination increase over time, which is not accounted for in Frössling-like equations.

Notation

a	specific interfacial area, L^2
c_B	surfactant bulk concentration, $M L^{-3}$
c^+	dimensionless surfactant concentration
CMC	critical micelle concentration, $M L^{-3}$
d^+	dimensionless length-scale
d_0	initial bubble diameter, L
D_i	bulk diffusivity of species, i, $L^2 T^{-1}$
$D_{s,i}$	interfacial diffusivity of species i, $L^2 T^{-1}$
g	gravity acceleration, $L T^{-1}$
k_L	mass transfer coefficient, $L T^{-1}$
$k_L a$	volumetric mass transfer coefficient, T^{-1}
Q	gas flow rate, $L^3 T^{-1}$
r_0	initial bubble radius (=orifice radius), L
R	universal gas constant, $M L^2 T^{-2} m^{-1} t^{-1}$
t	time, T
t^+	dimensionless time-scale
t_B	bubble age, T
T	absolute temperature, t
u	bubble rising velocity, $L T^{-1}$
V	volume of vessel, L^3
x_{O_2}	dissolved oxygen concentration, $M L^3$

Greek letters

α	ratio of process water $k_L a$ to pure water $k_L a$
γ	dynamic surface tension, $M T^2$
γ_0	solvent surface tension, $M T^2$
γ_∞	solvent equilibrium surface tension, $M T^2$
γ_∞^+	dimensionless equilibrium surface tension, $M T^2$
$\Delta\rho$	gas–liquid differential density, $M L^3$
Γ	dynamic interfacial accumulation, $m L^2$
Γ_∞	equilibrium dynamic interfacial accumulation, $m L^2$

Π_j	dimensionless groups, $j = 1, \ldots, 7$
ϕ	subsurface concentration, $\mathrm{M\,L^3}$

Dimensionless numbers

(Bd)	Bond number
$(Pe)_s$	interfacial Péclet number
(Re)	Reynolds number
(Ro)	interfacial contamination number
(Sc)	Schmidt number
$(Sh)_s$	interfacial Sherwood number
(Sm)	gravitational contamination number

Chemical species

IAA	iso-amyl alcohol
SDS	sodium dodecyl sulphate
TGT	sodium tetradecyl sulphate (Tergitol 4)

Acknowledgement

The authors thank Edward Ruth of the UCLA Henri Samueli School of Engineering and Applied Science for the invaluable technical support in troubleshooting the experimental setup.

Appendix A. Solution to the Ward–Tordai equation at short-time limits

The time-dependent diffusion-controlled dynamic interfacial adsorption kinetics at air-aqueous surfactant solutions was first quantified with an analytical equation by Ward and Tordai (1946). Their equation relates surfactant interfacial accumulation $\Gamma(t)$ with surfactant interfacial concentration and diffusivity for planar surfaces, accounting for surfactant back-movement to the subsurface (in the integral term). The subsurface is defined as the surface of the spherical region outside the semi-spherical forming bubble with diameter equal to the capillary (Fig. A.1). Following the procedure by Liu et al. (2004), the Ward and Tordai equation can be written in spherical coordinates by solving the diffusion equation

$$\frac{\partial c}{\partial t} = D_{\mathrm{SAA}} \nabla^2 c \tag{A.1}$$

which in spherical coordinates in a constant-diffusion system, where the only spatial variable is r, reduces to

$$\frac{\partial c(r,t)}{\partial t} = D_{\mathrm{SAA}} \frac{\partial^2 c(r,t)}{\partial r^2} + \frac{2D_{\mathrm{SAA}}}{r} \frac{\partial c(r,t)}{\partial r}, \tag{A.2}$$

assuming that the surfactant interfacial diffusivity is constant within the integration domain, and an intrinsic property of the chemical species, not a function of its concentration. Fig. A.1 illustrates a schematic of the gas-bubble formation and the integration domain of Eq. (A.2). The outer integration limit, the bubble subsurface, is the point at which the bubble will have maximum pressure, corresponding to the bubble having diameter equal to the capillary diameter. The initial and boundary conditions are:

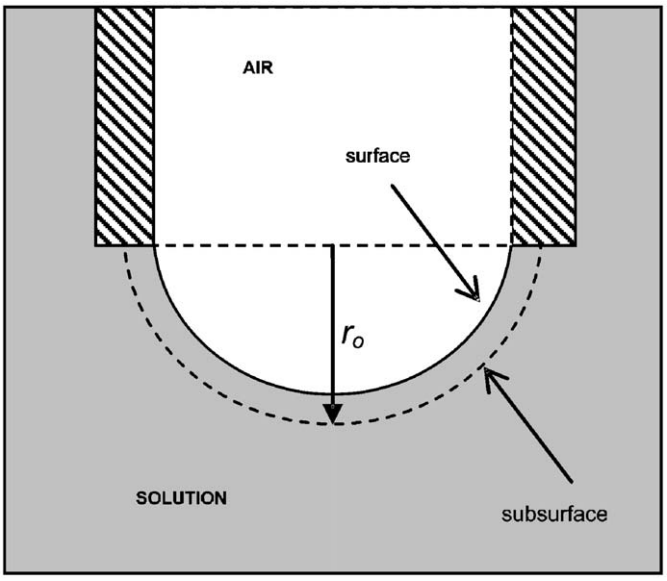

Fig. A.1. Domain of the Ward–Tordai equation at bubble formation.

$$c(r, 0) = c_B,$$

$$c(r \to \infty, t) = c_B,$$

$$c(r_0, t) = \phi(t). \tag{A.3}$$

By introducing the transform variable

$$w = c \cdot r, \tag{A.4}$$

Eq. (A.1) becomes

$$\frac{\partial w}{\partial t} = D_{\mathrm{SAA}} \frac{\partial^2 w}{\partial r^2}. \tag{A.5}$$

By defining

$$\tilde{w} = \int_0^\infty w \cdot \mathrm{e}^{-p \cdot t}\, \mathrm{d}t, \tag{A.6}$$

the conditions (A.3) become

$$w(r, o) = c_B \cdot r$$

$$w(r_0, t) = r_0 \cdot \phi \tag{A.7}$$

and the Laplace transform is:

$$\tilde{w} = r_0 \cdot [\phi(t) - c_B] \cdot \left[\frac{\mathrm{e}^{(r_0 - r)} \sqrt{p / D_{\mathrm{SAA}}}}{p} \right] + \frac{c_B \cdot r}{p}. \tag{A.8}$$

The solution to Eq. (A.2) is then

$$c(r,t) = c_B + [\phi(t) - c_B] \cdot \left(\frac{r_0}{r} \right) \cdot \mathrm{erfc}\left(\frac{r - r_0}{\sqrt{4 D_{\mathrm{SAA}} t}} \right) \quad (r \geqslant r_0) \tag{A.9}$$

or

$$c(r,t) = c_B + [\phi(t) - c_B] \cdot \left(\frac{r_0}{r}\right) + \frac{2[c_B - \phi(0)]}{\sqrt{\pi}} \cdot \left(\frac{r_0}{r}\right) \times \int_0^{r-r_0/\sqrt{4D_{SAA}t}} \exp(-z^2)\,dz - \frac{2}{\sqrt{\pi}}\frac{r_0}{r} \times \int_0^t \phi'(w) \left[\int_0^{r-r_0/\sqrt{4D_{SAA}t}} \exp(-z^2)\,dz\right] du \quad (A.10)$$

By applying Eq. (A.10) to Fick's first law

$$\left.\frac{\partial \Gamma(t)}{\partial t}\right|_{r_0} = \left.\frac{d\Gamma(t)}{dt}\right|_{r_0} = D_{SAA} \left.\frac{\partial c(r,t)}{\partial r}\right|_{r_0} \quad (4)$$

we obtain the solution in terms of surface contamination $\Gamma(t)$:

$$\Gamma(t) = \frac{D_{SAA} \cdot c_B \cdot t}{r_0} - \frac{D_{SAA}}{r_0} \cdot \int_0^t \phi(t)\,dt + 2\sqrt{\frac{D_{SAA}}{\pi}} \times \left\{c_B \cdot \sqrt{t} - \int_0^{\sqrt{t}} \phi(z)\,d[\sqrt{t-z}]\right\} \quad (A.11)$$

where c_B = surfactant bulk concentration (ML^{-3}), $\phi(t)$ = subsurface concentration (ML^{-3}), D_{SAA} = surfactant bulk diffusivity (L^2T^{-1}), and r_0 = initial bubble radius or the orifice radius (L).

There are numerous proposed simplifications of Eq. (A.11) for the short- and long-time adsorption cases (Hansen, 1960; Rillaerts and Joos, 1982; Daniel and Berg, 2001, 2003). The short-time behaviour is obtained by assuming a net migration of surfactants to the bubble, i.e. neglecting the integral terms which account for the backwards movement of solute (ϕ). At short-time adsorption limits it is therefore possible to calculate the surfactant interfacial accumulation $\Gamma(t)$ by considering the non-integral terms in Eq. (A.11) (Liu et al., 2004):

$$\Gamma(t) = \frac{D_{SAA} \cdot c_B \cdot t}{r_0} + 2c_B\sqrt{\frac{D_{SAA} \cdot t}{\pi}}. \quad (5)$$

The equation for long-time behaviour is derived by either expanding the integral at long times (Hansen limit, Hansen, 1960), or neglecting the change in interfacial surfactant concentration at long times, which allows it to be factored outside the integral (Joos limit, Rillaerts and Joos, 1982).

References

Acrivos, A., Goddard, J.D., 1965. Asymptotic expansions for laminar forced-convection heat and mass transfer—Part 1. Low speed flows. Journal of Fluid Mechanics 23, 273–291.

Alves, S.S., Orvalho, S.P., Vasconcelos, J.M.T., 2005. Effect of bubble contamination on rise velocity and mass transfer. Chemical Engineering Science 60, 1–9.

ASCE-American Society of Civil Engineers, 1984, 1991. Measurement of oxygen transfer in clean water. American Society of Civil Engineers—ASCE 2-91, 345 E. 47th St, New York.

ATV-DVWK Abwassertechnische Vereinigung-Deutsche Vereinigung für Wasserwirtschaft, Abwasser und Abfall e.V. 1996. Measurement in clean water and activated sludge of the oxygen transfer by aeration installations in activated sludge plants. Advisory Leaflet ATV-M 209 E, Deutsche Vereinigung für Wasserwirtschaft, Abwasser und Abfall e.V., Wuppertal.

Boussinesq, J., 1913. Vitesse de la chute lente, devenue uniforme, d'une goutte liquide sphérique, dans un fluide visqueux de poids spécifique moindre. Annales de Chimie et de Physique 29, 364–372.

Clift, R., Grace, J.R., Weber, M.E., 1978. Bubbles, Drops and Particles. Academic Press, New York.

Côté, P., Bersillon, J.-L., Huyard, A., 1989. Bubble-free aeration using membranes: mass transfer analysis. Journal of Membrane Science 47, 91–106.

Danckwerts, P.V., 1951. Significance of liquid-film coefficients in gas absorption. Industrial and Engineering Chemistry 43, 1460–1467.

Daniel, R.C., Berg, J.C., 2001. Diffusion-controlled adsorption at the liquid-air interface: the long-time limit. Journal of Colloid and Interface Science 237, 294–296.

Daniel, R.C., Berg, J.C., 2003. A simplified method for predicting the dynamic surface tension of concentrated surfactant solutions. Journal of Colloid and Interface Science 260, 244–249.

Datwani, S.S., Stebe, K.J., 2001. Surface Tension of an Anionic Surfactant: Equilibrium, Dynamics, and Analysis for Aerosol-OT. Langmuir 17, 4287–4296.

Eckenfelder, W.W., 1959. Absorption of oxygen fro air bubbles in water. Journal of the Sanitary Engineering Division, Proceedings of the American Society of Civil Engineers, 2090, pp. 89–99.

Eckenfelder, W.W., Barnhart, E.L., 1961. The effect of organic substances on the transfer of oxygen fro air bubbles in water. American Institute of Chemical Engineers Journal 7, 631–634.

Fainerman, V.B., Miller, R., Joos, P., 1994. The measurement of dynamic surface tensions of highly viscous liquids by the maximum bubble pressure method, colloids and surfaces A. Physiochemical and Engineering Aspects 75, 229–235.

Fan, L.-S., Tsuchiya, K., 1990. Bubble Wake Dynamics in Liquids and Liquid–Solid Suspensions. Butterworth-Heinemann, Boston.

Ferri, J.K., Stebe, K.J., 2000. Which surfactants reduce surface tension faster? A scaling argument for diffusion-controlled adsorption. Advances in Colloids and Interface Science 85, 61–97.

Freud, B.B., Freud, H.Z., 1930. A theory of the ring method for the determination of surface tension. Journal of the American Chemical Society 52, 1772–1782.

Friedlander, S.K., 1957. Mass transfer to single spheres and cylinders at low Reynolds numbers. American Institute of Chemical Engineers Journal 3, 43–48.

Frössling, N., 1938. Über die Verdunstung fallender Tropfen. Gerlands Beiträge zur Geophysik 52, 170–215.

Garner, F.H., Hammerton, D., 1954. Circulation inside gas bubbles. Chemical Engineering Science 3, 1–11.

Griffith, R.M., 1960. The effect of surfactants on the terminal velocity of drops and bubbles. Chemical Engineering Science 12, 198–213.

Haberman, W.L., Morton, R.K., 1953. An experimental investigation of the drag and shape of air bubbles rising in various liquids. D.W. Taylor Model Basin Report 802, Navy Department, Washington, DC.

Hansen, R.S., 1960. The theory of diffusion controlled absorption kinetics with accompanying evaporation. Journal of Physical Chemistry 64, 637–641.

Harkins, W.D., Jordan, H.F., 1930. A method for the determination of surface and interfacial tension from the maximum pull on a ring. Journal of the American Chemical Society 52, 1751–1772.

Higbie, R., 1935. The rate of absorption of a pure gas into a still liquid during short periods of exposure. American Institute of Chemical Engineers Transactions 31, 365–388.

Huo, D.L., 1998. The effect of dynamic surface tension on oxygen transfer coefficient in fine bubble aeration system. Ph.D. Thesis, University of California, Los Angeles.

Lamont, J.C., Scott, D.S., 1970. An Eddy cell model of mass transfer into the surface of a turbulent liquid. American Institute of Chemical Engineers Journal 16, 513–519.

Lecomte du Noüy, P., 1919. A new apparatus for measuring surface tension. Journal of General Physiology 1, 521–524.

Levich, V.G., 1962. Physicochemical Hydrodynamics. 2nd ed. Prentice-Hall, New York.

Lewis, W.K., Whitman, W.G., 1924. Principles of gas absorption. Industrial and Engineering Chemistry 16, 1215–1220.

Lin, J.N., Banerji, S.K., Yasuda, H., 1994. Role of interfacial tensions in the formation and the detachment of air bubbles. 2. A Single Orifice on an Inclined Plane Immersed in Water. Langmuir 10, 943–948.

Liu, J., Wang, C., Messow, U., 2004. Adsorption kinetics at air/solution interface studied by maximum bubble pressure method. Colloid and Polymer Science 283, 139–144.

Mancy, K.H., Okun, D.A., 1960. Effects of surface active agents on bubble aeration. Journal of the Water Pollution Control Federation 32, 351–364.

Marangoni, C., 1871. Über die Ausbreitung der Tropfen einer Flüssigkeit auf der Oberfläche einer anderen. Annalen der Physik und Chemie CXLII, 337–354.

Masutani, G.K., Stenstrom, M.K., 1991. Dynamic surface tension effects on oxygen transfer. Journal of Environmental Engineering 117, 126–142.

Miles, G.D., Shedlovsky, L., 1944. Minima in surface tension-concentration curves of solutions of sodium alcohol sulfates. Journal of Physical Chemistry 48, 57–62.

Motarjemi, M., Jameson, G.J., 1978. Mass transfer from very small bubbles—the optimum bubble size for aeration. Chemical Engineering Science 33, 1415–1423.

Philichi, T., Stenstrom, M.K., 1989. The effect of dissolved oxygen probe lag upon oxygen transfer parameter estimation. Journal of the Water Pollution Control Federation 61, 83–86.

Prandtl, L., 1934. Fundamentals of Hydro- and Aeromechanics. Tietjens, O.G. (Ed.), McGraw-Hill, New York.

prEN 12255-15-European Standard, 1999. Wastewater treatment plants—part 15: measurement of the oxygen transfer in clean water in activated sludge aeration tanks (Prédiction des capacités d'oxygénation en eau claire des systèmes d'insufflation d'air). NormAPME, Brussels.

Rillaerts, E., Joos, P., 1982. Rate of demicellization from the dynamic surface tension of micellar solutions. Journal of Physical Chemistry 86, 3471–3478.

Rosen, M.J., 1978. Surfactants and Interfacial Phenomena. Wiley, New York.

Rosso, D., 2005. Mass transfer at contaminated bubble interfaces. Ph.D. Thesis, University of California, Los Angeles.

Rosso, D., Iranpour, R., Stenstrom, M.K., 2005. Fifteen years of off-gas transfer efficiency measurements on fine-pore aerators: key role of sludge age and normalized air flux. Water and Environmental Research 77 (3), 266–273.

Sadhal, S.S., Johnson, R.E., 1983. Stokes-flow past bubbles and drops partially coated with thin—films. 1. Stagnant cap of surfactant film-exact solution. Journal of Fluid Mechanics 126, 237–250.

Sadhal, S.S., Ayyaswamy, P.S., Chung, J.N., 1997. Transport Phenomena with Drops and Bubbles. Springer, New York.

Vasconcelos, J.M.T., Orvalho, S.P., Alves, S.S., 2002. Gas–liquid mass transfer to single bubbles: effect of surface contamination. American Institute of Chemical Engineers Journal 48, 1145–1154.

Ward, A.F.H., Tordai, L., 1946. Time-dependence of boundary tensions of solutions I. The role of diffusion in time-effects. The Journal of Chemical Physics 14, 453–461.

Weber, M.E., 1975. The effect of surface active agents on mass transfer from spherical cap bubbles. Chemical Engineering Science 30, 1507–1510.

Zlokarnik, M., 1980. Koaleszenzphänomene im System gasförming/flüssig und deren Einfluß auf den O2-Eintrag bei der biologischen Abwassereinigung. Korrespondenz Abwasser 27, 728–734.

Zlokarnik, M., 2002. Scale-Up in Chemical Engineering. Wiley-VCH, Weinheim.